

Srinivasan S. Iyengar

## Ab initio dynamics with wave-packets and density matrices

Received: 14 April 2005 / Accepted: 11 August 2005 / Published online: 19 October 2005  
© Springer-Verlag 2005

**Abstract** Efficient methodologies to conduct simultaneous dynamics of electrons and nuclei are discussed. Particularly, attention is directed to a recent development that combines quantum dynamics with ab initio molecular dynamics. The two components of the methodology, namely, quantum dynamics and ab initio molecular dynamics, are harnessed together using a time-dependent self-consistent field-like coupling procedure. An approach to conduct quantum dynamics using an accurate banded, sparse and Toeplitz representation for the discrete free propagator is highlighted with suitable review of other related approaches. One notable feature of the method is that all important quantum dynamical effects including zero-point effects, tunneling as well as over-barrier reflections are accurately treated. Computational methodologies for improved efficiency of the quantum dynamics are also discussed. There exists a number of ways to carry out simultaneous ab initio molecular dynamics (such as Born–Oppenheimer dynamics and extended Lagrangian dynamics, Car–Parrinello dynamics being a prime example of the latter); our prime focus remains on atom-centered density-matrix propagation and Born–Oppenheimer dynamics. The electronic degrees of freedom are handled at accurate levels of density functional theory, using hybrid or gradient corrected approximations. Benchmark calculations are provided for a prototypical proton transfer system. Future generalizations and goals are discussed.

### 1 Introduction

The time-dependent Schrödinger equation is the starting point for many computational methodologies in gas-phase [1] and condensed-phase quantum dynamics [2]. Commonly, the Born–Oppenheimer approximation is invoked which allows propagation of nuclei, quantum-mechanically [1,3–26],

classically [27–31], or semi-classically [32–43] on fitted electronic surfaces or on “on-the-fly” [27–32,44–46] approximations to the same. For cases where fitted electronic surfaces are used, the required number of quantum chemical calculations to obtain a faithful representation of the surface can be very large depending upon the size of the system. It is in this regard that “on-the-fly” approaches to dynamics of nuclei and electrons [27–32,44–46] have recently become popular, leading to the sub-field of ab initio molecular dynamics (AIMD). The potential energy surfaces in both approaches may either be obtained from highly accurate, but demanding, electronic structure calculations or from parameterizations of the associated surfaces.

It should be noted that “on-the-fly” approaches to electron–nuclear dynamics are nearly as old as quantum mechanics itself (see for example Refs. [47,48] for a description of the Dirac–Frenkel time-dependent variational principle, which constitutes a formally exact “on-the-fly” dynamics scheme). More recently, many novel approaches to “on-the-fly” AIMD have been developed. Here, an approximation to the electronic wavefunction is propagated along with the nuclear degrees of freedom to simulate dynamics on the Born–Oppenheimer surface. If the nuclei are treated classically [29–31,44,45,49] then the forces on the nuclei are determined from the electronic structure. Perhaps all of these approaches can be broadly categorized into: (a) Born–Oppenheimer dynamics (BOMD) approaches, where the electronic structure is converged self-consistently, or (b) extended Lagrangian approaches [50,51], where an approximation to the electronic structure is propagated through an adjustment of the relative time scales of electrons and nuclei. The Car–Parrinello method [29,45,49] is a well-known example of the latter approach. The AIMD approaches when combined with full quantum or semiclassical dynamics schemes, has the potential to treat large problems accurately with the complete machinery of quantum dynamics. Several steps have been taken in this direction [32,52–55].

Our group [55–57] has recently developed a new approach that attempts to overcome some bottlenecks in this area. Our method combines full quantum-wave-packet

S. S. Iyengar  
Department of Chemistry and Department of Physics,  
Indiana University, 800 E. Kirkwood Ave, Bloomington,  
IN 47405, USA  
E-mail: iyengar@indiana.edu

dynamics treatment of the time-dependent Schrödinger equation with ab initio molecular dynamics. The latter is performed using Atom-centered Density-Matrix Propagation (ADMP) [31, 58] and Born–Oppenheimer molecular dynamics [27, 28, 30]. The wave-packet dynamics is performed through an analytic, banded, Toeplitz<sup>1</sup> approximation to the discretized free propagator [26, 59–63]. We have thus attempted an important synergy between formally accurate approaches in quantum scattering theory [1, 5, 6, 9, 10, 12, 22, 23, 36–38, 61, 64] and approximate ab initio molecular dynamics methods [27–31, 44, 46, 58, 65–69] to achieve efficient quantum dynamics of large systems. Some features of our approach include: (a) accurate treatment of the electronic degrees of freedom by including hybrid density functionals (for example B3LYP), (b) formally exact and efficient quantum propagation where the numerical description of the wave-packet adapts to the shape and position of the same to provide a flexible propagation scheme, (c) efficient treatment of large systems based on established linear scaling electronic structure techniques [70–72] and linear scaling quantum dynamical propagation with respect to grid basis size [55], and (d) established QM/MM generalization [57] for treatment of large systems. One notable feature of our approach is that all important quantum dynamical effects including zero-point effects, tunneling as well as over-barrier reflections are accurately treated.

The paper is organized as follows: In Sect. 2 we highlight the salient features of our theoretical formalism. This leads to a discussion of quantum wave-packet dynamics in Sect. 2.1 and the ADMP approach to dynamics of electrons and classical nuclei in Sect. 2.2. Approaches related to our formalism are reviewed in each section. Computational aspects of the methodology, including enhancement of efficiency, are discussed in Sect. 2.3. Section 3 deals with a discussion of the numerical results on a prototypical [38] system of important in condensed phase proton transfer as well as in weak acid-base chemistry [73]. In Sect. 4 we present some future goals and highlights for the methodology.

## 2 Wave-packet generalization for the atom-centered density-matrix propagation (ADMP) and Born–Oppenheimer dynamics schemes

To formulate an efficient dynamical methodology for large chemically reactive systems, we recognize that one may, in general, partition the full system based on chemical complexity. For example, some nuclei in chemical systems may require only classical treatment. Yet other parts of the system, including electrons or nuclei with relatively large de Broglie wavelengths, may need to be treated by applying full quantum dynamics or approximations to the same. If we assume that these individual parts of the full system interact

with each other in an average sense then we may employ a TDSCF-like [47, 74, 75] partitioning scheme where the full electron-nuclear system is divided into three parts: the first portion comprises a subsystem to be treated using quantum dynamics and the position variables for the particles in this part are denoted by  $R_{\text{QM}}$  in the discussion below. The second subsystem comprises most of the nuclear degrees of freedom and will eventually be treated within a classical framework (note that some nuclei may be included in the first part treated with quantum dynamics). The position variables for these particles are denoted by  $\mathbf{R}_C$ . The third portion comprises the electrons in the system. Based on the time-dependent Self-consistent field technique [47, 74–76] we can now reduce the full electron-nuclear time-dependent Schrödinger equation into three separate equations one describing each subsystem:

$$i\hbar \frac{\partial}{\partial t} \chi(R_{\text{QM}}; t) = \mathcal{H}_1 \chi(R_{\text{QM}}; t) \quad (1)$$

$$i\hbar \frac{\partial}{\partial t} \phi(\mathbf{R}_C; t) = \mathcal{H}_2 \phi(\mathbf{R}_C; t) \quad (2)$$

$$i\hbar \frac{\partial}{\partial t} \psi(r; t) = \mathcal{H}_3 \psi(r; t) \quad (3)$$

where  $\mathcal{H}_1$  is the average (or effective) Hamiltonian of system 1 and is written as  $\langle \phi \psi | \mathcal{H} | \phi \psi \rangle$  where  $\mathcal{H}$  is the full electron-nuclear Hamiltonian.  $\mathcal{H}_2$  and  $\mathcal{H}_3$  are similarly defined. It must be noted that Eqs. (1), (2) and (3) are obtained by writing the full wavefunction  $\Psi(r, R; t) \equiv \chi \phi \psi \exp[i\gamma]$ , where  $d\gamma/dt$  is proportional to twice the energy of the system. System 1 is to be treated quantum-dynamically. Since system 2 comprises nuclei that are not required to be treated within a quantum dynamical formalism, we may enforce the classical limit ( $\hbar \rightarrow 0$ ) for these particles [67, 77–87]. In system 3, which comprises electrons, we may enforce the space–time separation to obtain a stationary state description of electrons. In this fashion one recovers a formalism where a portion of the full system is treated using quantum dynamics, another portion of the system is treated classically, while a third portion (the electrons) is described within a stationary state approximation. In absence of system 2, the partitioning scheme described here reduces to the adiabatic approximation of electrons and nuclei which has been the cornerstone for many time-dependent as well as time-independent methods in quantum scattering theory [1].

An alternative approach is to treat the dynamics of systems 2 and 3 by employing “on-the-fly” AIMD techniques. Our implementation involves the recently developed ADMP formalism [31, 58, 65–69]. Here, the electronic structure is represented by a single particle electronic density matrix and is propagated simultaneously with the classical nuclei, with a simple adjustment of the relative nuclear and electronic time scales. The simultaneous dynamics is achieved within an extended Lagrangian formalism [29, 31, 50, 51, 58]. It has been shown that this dynamical strategy leads to a trajectory that oscillates about the Born–Oppenheimer surface with controllable deviations [58, 66] and the results agree well with Born–Oppenheimer dynamics calculations [65, 69]. ADMP has also been shown to be computationally superior to

<sup>1</sup> The  $(i, j)$ -th element of a Toeplitz matrix depends only on  $|i - j|$ . This property of the free propagator used in the current contribution yields an efficient scheme where only the first (banded) row of the matrix representation of the time-evolution operator needs to be stored.

Born–Oppenheimer dynamics, and this is on account of the relaxation of SCF convergence requirement in ADMP [65, 55, 68, 69]. The corresponding equations for the systems 2 and 3 are

$$\mathbf{M} \frac{d^2 \mathbf{R}_C}{dt^2} = - \left\langle \chi \left| \frac{\partial E(\{\mathbf{R}_C, \mathbf{P}_C\}, R_{QM})}{\partial \mathbf{R}_C} \right| \chi \right\rangle \quad (4)$$

and

$$\underline{\mu}^{1/2} \frac{d^2 \mathbf{P}_C}{dt^2} \underline{\mu}^{1/2} = - \left\langle \chi \left| \frac{\partial E(\{\mathbf{R}_C, \mathbf{P}_C\}, R_{QM})}{\partial \mathbf{P}_C} \right| \chi \right\rangle_{\mathbf{R}_C} - [\mathbf{\Lambda} \mathbf{P}_C + \mathbf{P}_C \mathbf{\Lambda} - \mathbf{\Lambda}]. \quad (5)$$

Here  $\mathbf{M}$  denotes the classical nuclear masses in system 2 and  $\underline{\mu}$  denotes a fictitious mass tensor or inertia tensor describing the effective electronic degrees of freedom.  $\mathbf{\Lambda}$  is a Lagrangian multiplier matrix used to impose N-representability of the single particle density matrix,  $\mathbf{P}_C$ . It is to be noted that Eq. (5) is classical in form, but not in content. Equations (4) and (5) are obtained by enforcing constraints of N-representability on the density matrix; the extended Lagrangian thus obtained:

$$\begin{aligned} \mathcal{L} = & \frac{1}{2} Tr(\dot{\mathbf{R}}_C^T \mathbf{M} \dot{\mathbf{R}}_C) + \frac{1}{2} Tr \left( \left[ \underline{\mu}^{1/4} \dot{\mathbf{P}}_C \underline{\mu}^{1/4} \right]^2 \right) \\ & - \langle \chi | \partial E(\{\mathbf{R}_C, \mathbf{P}_C\}, R_{QM}) | \chi \rangle \\ & - Tr[\mathbf{\Lambda}(\mathbf{P}_C \mathbf{P}_C - \mathbf{P}_C)], \end{aligned} \quad (6)$$

however, differs from that found in the standard time-dependent variational principle [47, 48] and is hence a fictitious Lagrangian. In Eq. (6),  $\dot{\mathbf{R}}_C$  and  $\dot{\mathbf{P}}_C$  are the nuclear and density matrix velocities. Further discussion on the associated fictitious dynamics of the electrons can be found in Section 2.2 with more details in Refs. [58, 66].

Equation (1) retains its original form and is given explicitly as:

$$\begin{aligned} i\hbar \frac{\partial}{\partial t} \chi(R_{QM}; t) \\ = \mathcal{H}_1 \chi(R_{QM}; t) \\ \equiv \left[ -\frac{\hbar^2}{2M_{QM}} \nabla_{R_{QM}}^2 + E(\{\mathbf{R}_C, \mathbf{P}_C\}, R_{QM}) \right] \chi(R_{QM}; t) \end{aligned} \quad (7)$$

The energy functional,  $E(\{\mathbf{R}_C, \mathbf{P}_C\}, R_{QM})$ , in Eqs. (4), (5) and (7), depends on the quantum particle coordinates,  $R_{QM}$ , the surrounding classical nuclear coordinates,  $\mathbf{R}_C$  and single particle electronic density matrix,  $\mathbf{P}_C$ , written in an orthonormal basis. The energy,  $E(\{\mathbf{R}_C, \mathbf{P}_C\}, R_{QM})$ , may be a density functional that involves exact exchange [88], a pure functional [89] (with gradient corrections [90] or higher order corrections [91–93]) or may be based on other single particle formalisms such as Hartree–Fock or semiempirical treatments. The energy in ADMP is written using McWeeny purification [94] for the density matrix,  $\tilde{\mathbf{P}}_C = 3\mathbf{P}_C^2 - 2\mathbf{P}_C^3$ :

$$E = Tr[\mathbf{h}\tilde{\mathbf{P}}_C + \frac{1}{2}\mathbf{G}(\tilde{\mathbf{P}}_C)\tilde{\mathbf{P}}_C] + E_{xc} + V_{NN}. \quad (8)$$

Here,  $\mathbf{h}$  is the one-electron matrix and  $\mathbf{G}(\tilde{\mathbf{P}}_C)$  is the Coulomb potential for DFT and the two-electron matrix for Hartree–Fock calculations.  $E_{xc}$  is the DFT exchange–correlation

functional (for Hartree–Fock  $E_{xc} = 0$ ) and  $V_{NN}$  represents the nuclear repulsion energy.

The formalism discussed here constitutes a quantum-classical partition scheme where a portion of the full system (subsystem  $R_{QM}$ ) is treated using full quantum dynamics while a different portion of the system (subsystem  $\mathbf{R}_C$ ) is treated using classical mechanics. The dynamics of the electrons, represented using the single particle density matrix  $\mathbf{P}_C$ , is either treated in a constrained classical-like fashion (Eq. (5)) or within the Born–Oppenheimer approximation. Quantum classical methods, however, have been known since the inception of quantum mechanics itself. For example, the first relationship between quantum and classical variables is due to Ehrenfest [95] who showed that the equation of motion for the average values of quantum observables coincides with the corresponding classical expression. The ideas of Madelung [78], de Broglie [79–82] and Bohm [83] exposed the fact that classical mechanics rigorously follows from quantum mechanics in the limit as  $\hbar \rightarrow 0$ . This aspect has been used by Gindensperger et al. [86] and Prezhdo *et al.* [87] to develop innovative quantum-classical schemes. A classical limit to quantum mechanics can also be obtained by considering the *disentanglement* [96, 97] of classical trajectories based on the Wigner phase space representation [98] of quantum mechanics.

In the subsections that follow we describe the different components of our methodology, *namely*, quantum dynamics in Sect. 2.1 and ab initio dynamics in Sect. 2.2. In Fig. 1 we present an illustration of the dynamics obtained using this methodology for a simple  $\text{Cl}^-\text{H}^+\text{Cl}^-$  system. The chloride ions are treated classically within the framework of AIMD while the shared proton is simultaneously treated using quantum dynamics. The electrons are treated using B3LYP density functional. On the left panel three separate potential energy surfaces are shown. These are potential energy surfaces that the quantum proton experiences at different instances during the dynamics. These potentials are different, since the chloride atoms are allowed to move according to ab initio dynamics. The three panels to the right have the appropriate potentials with corresponding wave-packet densities superimposed below. Hence, the quantum proton moves on an instantaneous surface created by the (moving) chloride atoms. The classical dynamics of the chloride ions is affected by the quantum proton and the electrons in the system. As can be seen the potential experienced by the quantum wave-packet can be very different at various instances in the dynamics process. For example, the potential here changes from a double well to single well and then back to a shallow double well. Furthermore, the wave-packet can split (or bifurcate) and this is the result of the exact quantum propagation to be discussed in Sect. 2.1. Figure 1 is shown to illustrate the dynamic nature of the interactions.

## 2.1 Quantum wave-packet propagation

In Refs. [55–57] the quantum-dynamical propagation is approximated using a kinetic reference symmetric split operator approach [5, 99]:

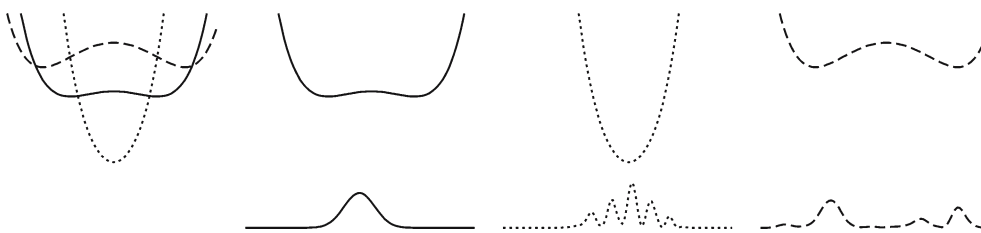


**Fig. 1** A brief illustration of the quantum wave-packet ab initio dynamics methodology for the  $\text{Cl}^- \text{H}^+$  system. The proton is treated using quantum dynamics and the chloride atoms and electrons follow ab initio dynamics. See text for details

$$\exp \left\{ -\frac{iHt}{\hbar} \right\} = \exp \left\{ -\frac{iVt}{2\hbar} \right\} \exp \left\{ -\frac{iKt}{\hbar} \right\} \exp \left\{ -\frac{iVt}{2\hbar} \right\} + \mathcal{O}(t^3) \quad (9)$$

where  $K$  is the kinetic energy operator of Eq. (7) and the  $V$  is the (local) potential energy operator. Operator splitting is a well-known concept in numerical solutions to partial differential equations where expressions similar to Eq. (9) are known as the Strang and Lie formulae [100]. In quantum mechanics these expressions are due to Trotter [5,99] and Nelson [101]. Equation (9) has the attractive feature that it provides dynamics strictly obeying time-reversal symmetry [5,99] provided the approximations used for the separate components of Eq. (9) are unitary. There exists a number of ways to proceed from this point. The important step is to recognize that for local potentials, the potential energy operator is diagonal in the coordinate representation. The free-propagator,  $\exp \left\{ -\frac{iKt}{\hbar} \right\}$  may be approximated in a number of ways. One approach is to recognize that this operator is diagonal in the momentum representation. Hence, fast Fourier transforms are commonly employed [5,8,16–19] to obtain the result of the free-propagator operating on a wave-packet in the coordinate representation. A few alternative approaches include: (a) the use of direct [22] or iterative, Lanczos [7] based diagonalization of the full Hamiltonian and the subsequent representation of the evolution operator  $\exp \left\{ -\frac{iHt}{\hbar} \right\}$  using the eigenstates, (b) the use of Chebychev polynomial approximations [6,11,20–22,102] (which are based on the Jacobi–Anger formula [103]), (c) use of eigenstates of various components of the Hamiltonian operator [104], and (d) the use of Feynman path integration [12–14,105,109]. The list here is not exhaustive and a detailed discussion on the topic may be found in Refs. [1,32]. In all cases, the Hamiltonian needs to be approximated in some representation. In the coordinate representation this is generally achieved with the discrete-variable representations (DVR) [23–25] or distributed approximating functionals (DAF) [59,60,63,110–112].

In our approach we employ an analytic banded distributed approximating functional (DAF) [59,61] representation for the coordinate space version of the free-propagator:

$$\left\langle R_{\text{QM}} \left| \exp \left\{ -\frac{iK \Delta t_{\text{QM}}}{\hbar} \right\} \right| R'_{\text{QM}} \right\rangle_{\text{DAF}} = \frac{1}{\sigma(0)} \exp \left\{ -\frac{(R_{\text{QM}} - R'_{\text{QM}})^2}{2\sigma(\Delta t_{\text{QM}})^2} \right\}$$

$$\times \sum_{n=0}^{M/2} \left( \frac{\sigma(0)}{\sigma(\Delta t_{\text{QM}})} \right)^{2n+1} \left( \frac{-1}{4} \right)^n \frac{1}{n!} (2\pi)^{-1/2} \times H_{2n} \left( \frac{R_{\text{QM}} - R'_{\text{QM}}}{\sqrt{2}\sigma(\Delta t_{\text{QM}})} \right), \quad (10)$$

where

$$\left\{ \sigma(\Delta t_{\text{QM}}) \right\}^2 = \sigma(0)^2 + \frac{i\Delta t_{\text{QM}}\hbar}{M_{\text{QM}}} \quad (11)$$

and  $H_{2n}(x)$  are the (complex) Hermite polynomials of even order. Equation (10) uses the well-known analytical expression for free evolution of a gaussian function [105],

$$\exp \left\{ -\frac{iK \Delta t_{\text{QM}}}{\hbar} \right\} \exp \left[ -\frac{x^2}{2\sigma(0)^2} \right] = \frac{\sigma(0)}{\sigma(\Delta t_{\text{QM}})} \exp \left[ -\frac{x^2}{2\sigma(\Delta t_{\text{QM}})^2} \right] \quad (12)$$

along with the fact that the Hermite functions are generated from gaussians according to

$$H_n(x) \exp \left[ -\frac{x^2}{2\sigma^2} \right] = (-1)^n \frac{d^n}{dx^n} \exp \left[ -\frac{x^2}{2\sigma^2} \right]. \quad (13)$$

Since the derivative operators  $\frac{d^n}{dx^n}$  commute with the free-propagator, the Hermite functions can be used as a basis to expand the exact quantum free propagator with coefficients as described in Eq. (10) [59]. This yields an efficient propagation scheme to perform quantum dynamics and Feynman path integration [105,106] through the action of a banded, sparse, Toeplitz matrix on a vector.

To understand the rationale behind the choice in Eq. (12) we provide a simplified derivation of this expression. Expanding the wave-packet at time  $t = 0$  using a local set of symmetric fitting functions,  $a(x - x_i)$ , we have

$$\chi(x; t = 0) = \sum_i \Delta x_i a(x - x_i) \chi(x_i; t = 0) \quad (14)$$

where  $\Delta x_i$  is the grid spacing (not in general uniform). The functions  $a(x - x_i)$  are *local* fitting functions the choice of which may in general depend upon the point  $x_i$ . One of the most common directions at this point is to assume that  $a(x - x_i) \equiv \delta(x - x_i) \equiv \langle x | x_i \rangle$  is a suitable approximation to the Dirac delta function. Subsequent resolution of the identity in terms of some complete set of basis functions leads to a representation of the wave-packet in that basis. The DAF

approximation differs from these approaches by assuming that a suitable *local* representation [59, 113] can be directly constructed for  $a(x - x_i)$ :

$$a(x - x_i) \equiv a_N(x - x_i; \sigma) = \sum_n^N b_n H_n \left( \frac{(x - x_i)}{\sqrt{2}\sigma} \right) \exp \left[ -\frac{(x - x_i)^2}{2\sigma^2} \right]. \quad (15)$$

Note that Eq. (15) is quite different from what will be obtained by using a standard basis set approximation for  $a(x - x_i)$  wherein the appropriate expression would be

$$a(x - x_i) \equiv \delta(x - x_i) = \sum_n \exp[-x^2/2] H_n(x) H_n(x_i) \times \exp[-x_i^2/2] \quad (16)$$

Note that Eq. (16) is separable in  $x$  and  $x_i$  whereas Eq. (15) only depends on  $(x - x_i)$ . The *local spectral* [114] form in Eq. (15) has many computational advantages not the least of which is the fact that the approximation to a propagator based on Eq. (15) yields a banded matrix at *any* level of approximation. The choice of Hermite functions here is by no means a requirement; it is however a convenient choice based on Eqs. (12) and (13). Using the orthogonality of the Hermite functions and the fact that  $a(x - x_i)$  must be symmetric with respect to interchange of  $x$  and  $x_i$  (since it approximates the Dirac delta function), one obtains

$$b_{2n+1} = 0 \quad (17)$$

$$b_{2n} = \frac{1}{\sigma\sqrt{2\pi}} \left(-\frac{1}{4}\right)^n \frac{1}{n!}$$

where we have used the identity [115]

$$\int dx \exp[-x^2] H_n(x) H_m(x) \equiv \delta_{n,m} 2^m m! \sqrt{\pi} \quad (18)$$

The free propagation of the wave-packet is then given by:

$$\begin{aligned} \chi(x; t) &= \exp \left\{ -\frac{iKt}{\hbar} \right\} \chi(x; t=0) \\ &= \exp \left\{ -\frac{iKt}{\hbar} \right\} \sum_i \Delta x_i a(x - x_i) \chi(x_i; t=0) \\ &= \exp \left\{ -\frac{iKt}{\hbar} \right\} \sum_i \Delta x_i \left\{ \sum_n b_{2n} H_{2n} \left( \frac{x - x_i}{\sqrt{2}\sigma} \right) \right. \\ &\quad \times \exp \left[ -\frac{(x - x_i)^2}{2\sigma^2} \right] \left. \right\} \chi(x_i; t=0) \\ &= \sum_i \Delta x_i \left\{ \sum_n b_{2n} \frac{\sigma(0)}{\sigma(\Delta t_{QM})} \right. \\ &\quad \times H_{2n} \left( \frac{x - x_i}{\sqrt{2}\sigma(\Delta t_{QM})} \right) \exp \left[ -\frac{(x - x_i)^2}{2\sigma(\Delta t_{QM})^2} \right] \left. \right\} \\ &\quad \times \chi(x_i; t=0), \end{aligned} \quad (19)$$

where we have used the fact that  $K$  acts only in  $x$  and have chosen  $\sigma \equiv \sigma(0)$ . Using Eq. (17), we recover the expression

in Eq. (10) as a suitable approximation for the discretized quantum propagator. There exists similarities between Eq. (10) and the wavelet theory of multi-resolution analysis and these have been discussed in detail elsewhere [69, 112, 114]. This is due to the differences between Eqs. (15) and (16).

As a consequence of the above discussion, it follows that

$$\begin{aligned} \chi(R_{QM}^i; t + \Delta t) &= \frac{\Delta x}{\sigma(0)} \sum_j \exp \left\{ -\frac{(R_{QM}^i - R_{QM}^j)^2}{2\sigma(\Delta t_{QM})^2} \right\} \\ &\quad \times \sum_{n=0}^{M/2} \left( \frac{\sigma(0)}{\sigma(\Delta t_{QM})} \right)^{2n+1} \\ &\quad \times \left( \frac{-1}{4} \right)^n \frac{1}{n!} (2\pi)^{-1/2} \\ &\quad \times H_{2n} \left( \frac{R_{QM}^i - R_{QM}^j}{\sqrt{2}\sigma(\Delta t_{QM})} \right) \chi(R_{QM}^j; t), \end{aligned} \quad (20)$$

where  $\Delta x$  is assumed uniform in this case and the propagation is expressed for a one-dimension system. Generalization to higher dimensions is straightforward and is carried out by writing the propagator in direct product form with components as in Eq. (10). The variables  $M$  and  $\sigma(0)$  determine the accuracy and width (or computational efficiency) respectively of the DAF. It has been shown [55, 59, 63] that these parameters are not independent and for a given value of  $M$  there exists a  $\sigma(0)$  that provides optimal accuracy for the propagation. The accuracy of this method in conjunction with ab initio dynamics has been benchmarked in Ref. [55].

We finally note that the method presented here differs from other approaches that use Hermite functions to represent the wavepacket [41, 116] based on Heller's Gaussian wavepacket formalism [36]. Within these formalisms [41, 116] a locally harmonic approximation to the potential [36] allows the reduction of the time-dependent Schrödinger equation to classical-like equations to propagate the width and center of the Gaussian wavepackets. In our case, no assumption is made on the nature of the potential and Hermite functions are used as part of the simplification resulting from Eqs. (12) and (13). In this sense the approach discussed here has connections to Feynman path integrals; indeed Eq. (10) may be considered as a Feynman path integral written in Hermite function representation.

### 2.1.1 A few comments on the DAF-wave-packet propagation scheme

It is worth noting a few characteristics of Eq. (10). For an approximation controlled by choice of parameters  $M$  and  $\sigma(0)$ , Eq. (10) only depends on the quantity  $(R_{QM} - R'_{QM})$ , that is distance between points in the coordinate representation, and goes to zero as this quantity becomes numerically large due to the Gaussian prefactor. This yields a banded matrix approximation to Eq. (10), for any  $M$  and  $\sigma(0)$ . Furthermore, on account of its dependence on  $(R_{QM} - R'_{QM})$ ,

a matrix representation of Eq. (10) has the property that all diagonal elements of this matrix are equal; similarly all  $n$ th super (and sub) diagonal elements are the same. Such a matrix is called a Toeplitz matrix. The dependence on  $(R_{\text{QM}} - R'_{\text{QM}})$  also implies a translational symmetry reminiscent of wavelet theories [117–120]. Hence, Eq. (10) provides great simplicity in computation of quantum propagation within our scheme and is expected to be useful for large systems. For example, it is only necessary to store the first row of such a matrix, in each dimension, to obtain the result of a propagation. The computational scaling of the quantum propagation described in Eq. (20) is  $\{(2W + 1)(N - W) - W^2\}$ , where  $N$  is the number of grid points used in the discretization scheme and  $(2W + 1)$  is the width of the propagator in the coordinate representation. Since  $W$  does not depend on  $N$  ( $W$  in fact depends on  $M$  and  $\sigma(0)$ , that is the required accuracy of propagation), this scaling goes as  $\mathcal{O}(N)$  for large grids.

The envelope of the DAF-propagator is proportional to the time-step [55], when the order of the approximation (determined by the choice of  $M$  and  $\sigma(0)$ ) is maintained. This is particularly interesting since our approach allows for an adaptive control of quantum timesteps, based on energy conservation, and in such cases when the timestep is increased more points in the vicinity of  $\chi(x)$  contribute to its propagation. Further the momentum space form of the DAF-propagator is a polynomial multiplied by a coherent state,  $\exp\left\{-\frac{k^2\sigma(\Delta t_{\text{QM}})^2}{4}\right\} \equiv \exp\left\{-\frac{k^2}{4}(\sigma(0)^2 + i\Delta t_{\text{QM}}\hbar/M_{\text{QM}})\right\}$ . The plane wave frequency in the coherent state is time-step dependent which implies that for larger time steps but fixed  $M$  and  $\sigma(0)$  the plane-wave portion of the Fourier transform of Eq. (10) becomes oscillatory for a given  $k$ . This is particularly interesting since coherent states have been used to propagate quantum systems [121–124], but in our case the propagator in the momentum representation is a coherent state multiplied by a polynomial.

## 2.2 Ab Initio dynamics using ADMP and Born–Oppenheimer dynamics

Equations (4) and (5), can be derived using the classical stationary conditions of action [125] on an extended Lagrangian, Eq. (6), that differs from that used in standard ADMP [31, 58, 65–69]. The resultant equations of motion, (4) and (5), are propagated using the velocity Verlet algorithm:

$$\begin{aligned} \mathbf{P}_C^{i+1} &= \mathbf{P}_C^i + \dot{\mathbf{P}}_C^i \Delta t - \frac{\Delta t^2}{2} \underline{\mu}^{-1/2} \\ &\times [\mathcal{F}_{\mathbf{P}_C}^i + \Lambda_i \mathbf{P}_C^i + \mathbf{P}_C^i \Lambda_i - \Lambda_i] \underline{\mu}^{-1/2}, \end{aligned} \quad (21)$$

$$\begin{aligned} \dot{\mathbf{P}}_C^{i+1} &= \dot{\mathbf{P}}_C^i - \frac{\Delta t}{2} \underline{\mu}^{-1/2} [\{\mathcal{F}_{\mathbf{P}_C}^i + \Lambda_i \mathbf{P}_C^i + \mathbf{P}_C^i \Lambda_i - \Lambda_i\} \\ &+ \{\mathcal{F}_{\mathbf{P}_C}^{i+1} + \Lambda_{i+1} \mathbf{P}_C^{i+1} + \mathbf{P}_C^{i+1} \Lambda_{i+1} - \Lambda_{i+1}\}] \underline{\mu}^{-1/2}, \end{aligned} \quad (22)$$

with

$$\mathcal{F}_{\mathbf{P}_C}^i = \left\langle \chi \left| \frac{\partial E(\{\mathbf{R}_C, \mathbf{P}_C\}, R_{\text{QM}})}{\partial \mathbf{P}_C} \right|_{\mathbf{R}_C} \right| \chi \rangle. \quad (23)$$

Similarly, the nuclei are propagated according to

$$\mathbf{R}_C^{i+1} = \mathbf{R}_C^i + \dot{\mathbf{R}}_C^i \Delta t - \frac{\Delta t^2}{2} \mathbf{M}^{-1/2} \mathcal{F}_{\mathbf{R}_C}^i \mathbf{M}^{-1/2}, \quad (24)$$

$$\dot{\mathbf{R}}_C^{i+1} = \dot{\mathbf{R}}_C^i - \frac{\Delta t}{2} \mathbf{M}^{-1/2} [\mathcal{F}_{\mathbf{R}_C}^i + \mathcal{F}_{\mathbf{R}_C}^{i+1}] \mathbf{M}^{-1/2}, \quad (25)$$

where

$$\mathcal{F}_{\mathbf{R}_C}^i = \left\langle \chi \left| \frac{\partial E(\{\mathbf{R}_C, \mathbf{P}_C\}, R_{\text{QM}})}{\partial \mathbf{R}_C} \right|_{\mathbf{P}_C} \right| \chi \rangle. \quad (26)$$

The velocity Verlet algorithm is obtained from a third-order Trotter factorization of the classical Liouillian and comprises a propagation scheme that preserves the Poincare integral invariants [125] of classical mechanics. This kind of a factorization retains consistency between the classical and quantum subsystem, since the symmetric split operator scheme for quantum propagation, i.e., Eq. (9), is also a third-order Trotter factorization of the *quantum* time-evolution operator.

If Born–Oppenheimer dynamics is to be used instead of ADMP, Eq. (5) is replaced by SCF convergence of  $\mathbf{P}_C$ . The nuclear propagation equation remains the same in both formalisms. However, the nuclear forces are different since ADMP nuclear forces are more general than the standard Born–Oppenheimer dynamics nuclear forces [31, 66] and the difference between these is proportional to the commutator of the Fock and density matrices [66] that is generally small in Born–Oppenheimer dynamics (when the SCF convergence threshold is tight) but may not be small in ADMP. Similarly, the density matrix gradient in Eq. (5) and (23) are also proportional to the commutator of the Fock and density matrix [31].

### 2.2.1 A few comments on ADMP

While our approach [55] maintains the flexibility to allow both extended Lagrangian as well as Born–Oppenheimer propagation of electrons, we must note that current implementation of the ADMP approach is computationally superior to Born–Oppenheimer dynamics [65] while retaining similar accuracy for appropriate choice of  $\underline{\mu}$ . This important advantage is critical in obtaining a practically viable scheme to perform electron-nuclear [56] as described here. The computational differences between Born–Oppenheimer and ADMP dynamics have discussed in detail in Refs. [55, 65].

The ADMP Eq. (5) is similar to that used in the Car–Parrinello (CP) scheme however, differs in using the single particle density matrix in an orthonormal basis set formed from Gaussian basis functions. In this sense Eq. (5) represents fictitious dynamics (like CP), where the density matrix

is propagated instead of being converged. The accuracy and efficiency of ADMP is controlled by the choice of  $\underline{\mu}$ . Hence one must be aware of the limits on this quantity. Two criteria [58,66] have been derived to place bounds on the choice of the fictitious mass. Firstly, the choice of the fictitious mass determines the magnitude of the commutator  $[\mathbf{P}_C, \mathbf{F}]$  thus determining the extent of deviation from the Born–Oppenheimer surface: [66]

$$\|[\mathbf{F}, \mathbf{P}_C]\|_F \geq \frac{1}{\|[\mathbf{P}_C, \dot{\mathbf{P}}_C]\|_F} \left| \text{Tr} \left[ \dot{\mathbf{P}}_C \underline{\mu}^{1/2} \ddot{\mathbf{P}}_C \underline{\mu}^{1/2} \right] \right| \quad (27)$$

where  $\|[\dots]\|_F$  is the Frobenius norm [126,127] of the commutator and is defined as  $\|A\|_F = \sqrt{\sum_{i,j} A_{i,j}^2}$ .  $\dot{\mathbf{P}}_C$  and  $\ddot{\mathbf{P}}_C$  are *velocity* and *acceleration* of the density matrix and can be determined on the fly as outlined in the propagation scheme described below. Secondly, the rate of change of the fictitious kinetic energy,

$$\begin{aligned} \frac{d\mathcal{H}_{fict}}{dt} &= \text{Tr} \left[ \dot{\mathbf{P}}_C \underline{\mu}^{1/2} \ddot{\mathbf{P}}_C \underline{\mu}^{1/2} \right] \\ &= -\text{Tr} \left[ \dot{\mathbf{P}}_C \left( \left. \frac{\partial E(\mathbf{R}, \mathbf{P})}{\partial \mathbf{P}} \right|_{\mathbf{R}} + \Lambda \mathbf{P} + \mathbf{P} \Lambda - \Lambda \right) \right], \end{aligned} \quad (28)$$

is *required to be bounded and oscillatory* and this again is determined by the choice of fictitious mass tensor. Note that the numerator in Eq. (27) is the same as the expression in Eq. (28) and hence this implies that the rate of change of the fictitious kinetic energy in ADMP is also proportional to the commutator  $[\mathbf{P}_C, \mathbf{F}]$  and hence determines deviations from the Born–Oppenheimer surface. One must monitor the quantities in Eqs. (27) and (28) to ascertain that the ADMP portion of the dynamics is physically consistent. In addition we require that the fictitious mass be chosen so that the density oscillations are an order of magnitude higher than the highest frequency nuclear motions [65] In all ADMP applications studied to date [31,58,65,68,128–130] these conditions are satisfied thus yielding a computationally efficient and accurate approach to model dynamics on the Born–Oppenheimer surface. It has been shown that ADMP trajectories thus obtained are in good agreement with dynamics on the Born–Oppenheimer surface [65,69]. Several interesting problems [65,68,69,128,129] have been studied using ADMP; perhaps the most notable among these include (a) a recent demonstration [128] that dynamical effects are critical in obtaining good infrared spectroscopic properties of flexible systems in agreement with experiment, (b) the prediction of the “amphiphilic” nature of the hydrated proton [128–130] in water clusters.

### 2.3 Computational details

The algorithm to perform the simultaneous dynamics of the  $\{\mathbf{R}_C, \mathbf{P}_C, \chi\}$  system is described as follows: First a grid is created around the particle to be treated quantum dynamically. This grid represents the discretization of the wave-packet,  $\chi$ , in the coordinate representation. If ADMP dynamics is

chosen, the potential energy  $E(\{\mathbf{R}_C, \mathbf{P}_C\}, R_{QM})$ , the nuclear forces,  $\left. \frac{\partial E(\{\mathbf{R}_C, \mathbf{P}_C\}, R_{QM})}{\partial \mathbf{R}_C} \right|_{\mathbf{P}_C}$  and density matrix forces,  $\left. \frac{\partial E(\{\mathbf{R}_C, \mathbf{P}_C\}, R_{QM})}{\partial \mathbf{P}_C} \right|_{\mathbf{R}_C}$ , are calculated on the grid points. On the contrary if Born–Oppenheimer dynamics is the chosen approach, then the potential energy and only classical nuclear forces are obtained based on SCF convergence. This is an important difference and clearly indicates the lower computational effort required in ADMP.

The potential energy on the grid along with the free propagator in Eq. (10) are then used for causal propagation of the quantum wave-packet. The energy gradients on the grid points are used along with the wave-packet to construct the force on the ADMP system as required by Eqs. (23) and (26), which propagates the ADMP variables:  $\{\mathbf{R}_C, \mathbf{P}_C\}$  and the associated velocities  $\{\dot{\mathbf{R}}_C, \dot{\mathbf{P}}_C\}$ , as allowed by Eqs. (21), (22), (24) and (25). Only the nuclear degrees of freedom are propagated for the Born–Oppenheimer case. This process is then repeated for the next propagation step.

The above algorithm is limited by the size of the quantum grid and to facilitate maximum compactness two procedures are currently implemented: (a) we use an adaptive grid procedure wherein new grid positions are recalculated every few timesteps based on the center and instantaneous distribution of the wave-packet. The wave-packet amplitudes at the new grid positions are calculated with an accurate grid interpolation scheme [110,60,131–133] to transform the wave-packet from old set of grid points to a new set. This way the quantum grid adapts to the region where the quantum wave-packet has significant contributions. (b) It is also important to note that the size of the quantum grid is closely related to the computationally expensive portion of the algorithm since it determines the number of energy and force evaluations to be performed as per Eqs. (8), (26) and (23). These computations are performed on the quantum grid points and used for ab initio dynamics. This necessitates a reduction of the number of grid points where such calculations are performed, without serious loss in accuracy. We have implemented a novel importance sampling approach that allows reduction of the number of grid points by nearly a factor of 10 per dimension [56] of quantum propagation. The sampling algorithm involves the determination of the importance level of a certain grid point based on the potential, grid projected gradient of potential and wave-packet density at the grid point [56]. This when coupled with subsequent interpolation yields a procedure that is robust, efficient, accurate and works “on-the-fly” to compress, instantaneously, the number of grid points requiring quantum-chemical calculations. The approach is seen to have many important advantages for use in propagation of multiple quantum particles in full dimensionality, which will be subject of future studies.

Another important factor in the quantum propagation scheme is related to the nature of the discretized DAF-propagator in Eq. (20). Equation (20) may be interpreted as a matrix–vector multiplication where the  $(R_{QM}^i, R_{QM}^j)$ th element of the propagator matrix acts on the initial vector to

create a new vector. In this case, we note that for points near the edges of the grid defined by  $[i \leq W]$  and  $[N - i \leq W]$ , where  $R_{\text{QM}}^i \equiv i \Delta x$ ,  $N$  is the number of grid discretization points and  $(2W + 1)$  is the width of the DAF-propagator in the coordinate representation, there is an error in the discretization scheme in Eq. (20) since  $\langle R_{\text{QM}}^i | \exp\left\{-\frac{iK \Delta t_{\text{QM}}}{\hbar}\right\} | R_{\text{QM}}^j \rangle_{\text{DAF}}$  is nonzero for  $[i \leq W]$  and  $j < 0$ . That is, the DAF-propagator extends beyond the region of definition of the grid. However, the size of this extended region is proportional to  $W \Delta x$ . One of the properties of the DAF-propagator is that its band width,  $W$ , is independent of the grid size  $\Delta x$  as long as the values of  $\sigma(0)$  and  $M$  are kept constant [133]. Hence, as  $\Delta x$  is made smaller, the total number of grid points,  $N$ , increases and the ratio  $W/N$  ( $\propto \Delta x$ ) gets smaller. Hence, as the grid spacing is reduced, the size of the extended region described above gets smaller and in the continuous limit, i.e., as  $\Delta x$  becomes infinitesimally small, this region,  $W/N \propto \Delta x$ , becomes infinitesimally small. For finite size grid spacings the numerical effects of this problem at grid boundaries is reduced by using Neumann boundary conditions [134] along with a symmetry-adapted version of the propagator. By contrast the current implementation uses Dirichlet-type boundary conditions.

### 3 Scattering amplitudes, quantum/classical correlated motion and evaluation of density functionals for proton transfer problems

An exhaustive study of the accuracy and efficiency of the dynamical methodology, including evaluation of the DAF parameters and comparisons between ADMP and Born–Oppenheimer wave-packet implementations have been carried out in Ref. [55]. Furthermore, performance of the approach with regards to quantum zero point effects, tunneling and over-barrier reflection has been fully evaluated [55]. It must be noted that most methodologies that study quantum dynamics in large systems do not adequately reproduce all three effects. While many methods accurately reproduce the zero-point effects, few are able to reproduce both tunneling and over-barrier reflection accurately. It is also worthwhile to note that standard semiclassical approximations (such as WKB [77]) break down in the vicinity of barrier height, which provides an initiative for a full quantum treatment. Our scheme was found [55] to accurately reproduce all three quantum dynamical effects described above. The scaling of errors in our algorithm is found to be proportional to  $\mathcal{O}(\Delta t^3)$  and this comes as no surprise on account of the third order Trotter factorization used in Eq. (9) and is implicit in the velocity Verlet equations (21), (22), (24) and (25). This however also proves that there are no additional spurious errors in our approach.

To illustrate the scalability of our approach with system size, we briefly describe here the proton transfer in a phenol-trimethylamine (see Fig. 2). This system has been considered prototypical for condensed phase proton transfer [38]. In addition, similar systems have been recently studied to

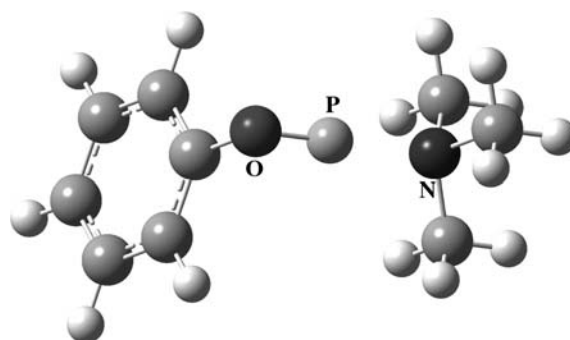


**Fig. 2** The phenol-amine system. The shared proton, the oxygen of the phenol and the nitrogen in the amine are marked. The shared proton is studied using wave-packet dynamics and the rest of the system is treated using ADMP

understand the quantum nuclear effects involved in the slow deprotonation step of weak acid-base chemistry [73]. These studies [73], however, use Marcus' theory [135] to obtain quantum corrections to the proton transfer process. We demonstrate the power of our approach in contributing significantly to such studies by treating the electronic effects accurately within hybrid DFT; in addition full quantum dynamical effects of the hopping proton are accurately treated within the wave-packet formalism. As outlined previously, these quantum effects may include zero-point effects, tunneling as well as over-barrier reflection. Our approach is capable of handling all three effects.

Phenol-trimethylamine is a classic case where the loss of the proton from the phenol is coupled to the delocalization of electrons in the ring. The electronic structure is thus treated using both B3LYP and BLYP density functionals as a demonstration. From our study we obtain the change in scattering matrix elements (for the proton transfer) with respect to initial wave-packet energy for both B3LYP and BLYP treatment of electronic degrees of freedom. We also study the effect of the phenol ring on the dynamics of the quantum proton.

In Fig. 3a we provide the wave-packet survival time in the reactant channel,  $\langle \chi_0 | \chi(t) \rangle$  and its half Fourier transform:

$$\int_0^{\infty} dt \exp\{iEt/\hbar\} \langle \chi_0 | \chi(t) \rangle \equiv \lim_{\epsilon \rightarrow 0} \left\langle \chi_0 \left| \frac{-i\hbar}{E - H + i\epsilon} \right| \chi_0 \right\rangle = \langle \chi_0 | G^+(E) | \chi_0 \rangle. \quad (29)$$

is provided in Fig. 3b. The operator  $G^+(E) \equiv [\lim_{\epsilon \rightarrow 0} -i\hbar (E - H + i\epsilon)^{-1}]$  is the causal Green's function. It has been shown [12, 61] that such a half Fourier transform is directly proportional to the scattering matrix element obtained from the S-matrix Kohn variational principle [64]. Figures 3a and 3b reveal marked differences between S-matrix element obtained from B3LYP and BLYP functionals, especially for intermediate scattering energies. For example, the S-matrix element at an energy of approximately  $2,000 \text{ cm}^{-1}$  is three times as much for BLYP as it is for B3LYP. Important differences are also seen in the survival time in the intermediate time region. In this region of intermediate time, the proton is partially bound to both phenol and amine and in such



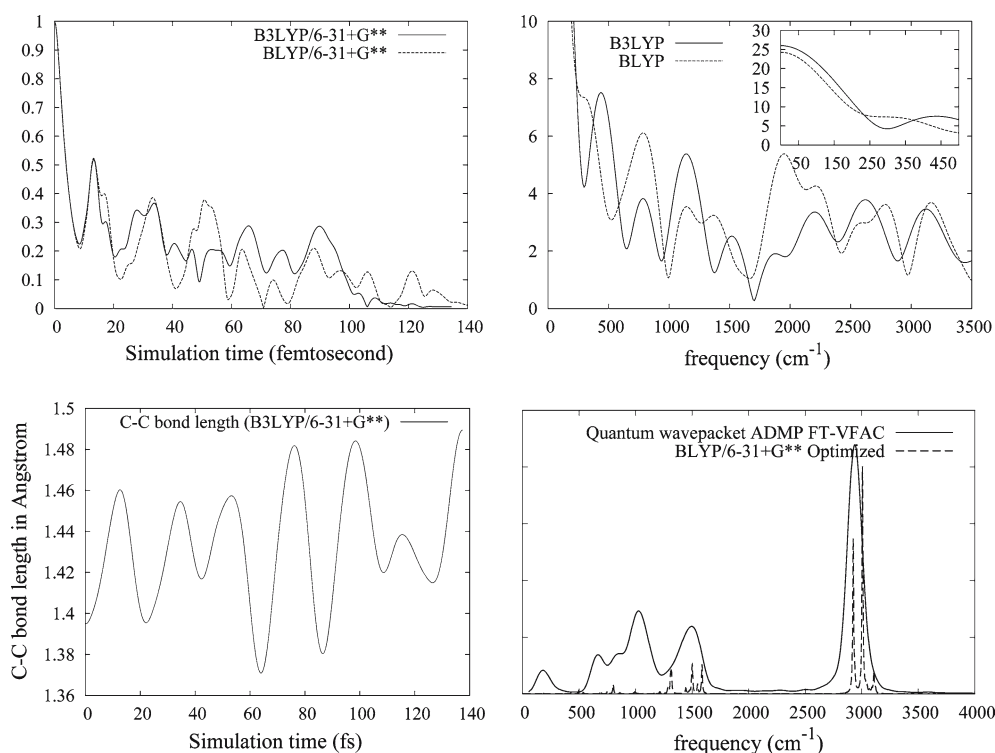


**Fig. 3** The quantity  $\langle \chi_0 | \chi(t) \rangle$  as a function of simulation time in (a) determines the survival of the wave-packet in the reactant channel. The half-Fourier transform of  $\langle \chi_0 | \chi(t) \rangle$  in (b) is directly proportional to the scattering matrix elements obtained from S-matrix Kohn variational principle [61]. The insert in (b) indicates the behavior for low scattering energies. In Fig. (c) we present the time-evolution of a C–C bond length during this simulation. As can be seen there is a correlation between this bond length and the oscillations in wave-packet evolution. See text for details. In Fig. (d) we present the correlation function from Eq. (30) along with frequencies obtained from a single point optimized BLYP calculation.

situations B3LYP and BLYP have been previously noted [68, 129] to provide significantly different results. (See Refs. [68, 129] where B3LYP and BLYP provide different hopping rates for proton translocation across a water wire in a Gramicidin A ion channel and in medium sized protonated water clusters.) From our treatment, we see that these differences in the intermediate time region lead directly to a discrepancy in the S-matrix obtained from the two functionals. Dynamical quantities such as transition probabilities and scattering matrix elements could, thus, be substantially different between the hybrid B3LYP and pure BLYP functionals when nuclear quantization is fully exploited. Thus accurate treatment of the surrounding electrons could be critical when treating proton transfer problems.

In Fig. 3c we also present the evolution of one of the carbon–carbon bond distances in the phenol system. The time-period of these oscillations is about 20 fs. Upon closer inspection of the the evolution of the quantity  $\langle \chi_0 | \chi(t) \rangle$  in Fig. 3a it is seen that this quantity also displays a period of approximately 20 fs at the beginning. (The oscillations are close to being out of phase by a factor of  $\pi$ .) This indicates a correlated motion between the carbon–carbon bond and the quantized proton and can be rationalized based on the fluctuations in the electrostatic interaction between the  $\pi$  electrons of the phenol and the quantized proton as a result of the breathing mode. It is clear that such an examination is

possible using the current methodology on account of rigorous quantum dynamical treatment in conjunction with accurate electronic structure. Future studies will include solvent effects through QM/MM generalization of the procedure described here.

To obtain the vibrational density of states from dynamics, the Fourier transform of the velocity–velocity autocorrelation is commonly used since it approximates the vibrational density of states. This aspect has been widely used in classical dynamics [136] as well as ab initio molecular dynamics [128]. In our case, the existence of classical as well as quantum-dynamically treated nuclei complicates the application of this concept. To study the effect of quantum dynamical treatment of the shared proton on the vibrational density of states, we have constructed the Fourier transform of the unified velocity–velocity, flux–flux autocorrelation function (FT-VFAC) [56]

$$C(\omega) = \int_{-\infty}^{+\infty} \exp[-i\omega t] \{ \langle v(t)v(0) \rangle_C + \langle \mathbf{J}(t)\mathbf{J}(0) \rangle_Q \} \quad (30)$$

where the average flux,  $\mathbf{J}(t)$ , of the quantum wavepacket is

$$\mathbf{J}(t) = \langle \mathcal{J} \rangle = \mathcal{R} \left[ \left\langle \psi(t) \left| \frac{-i\hbar}{2m} \nabla \right| \psi(t) \right\rangle \right]. \quad (31)$$

$\mathcal{R}[A]$  represents the real part of the complex number  $A$ . The symbols  $\langle \dots \rangle_C$  and  $\langle \dots \rangle_Q$  in Eq. (30) represent the classical and quantum variables ensemble averages. Here, we have exploited the connection between the probability flux and velocity and, in fact, the probability flux is the quantum correspondence to the velocity as is clear from the appearance of the momentum operator,  $[-i\hbar\nabla]$ , in Eq. (31). Equation (31), however, represents an “average-flux” for the quantum system. Our results are presented in Fig. 3(d) where optimized single point frequencies are also shown. While the latter includes only the harmonic frequency corresponding to a single optimized geometry, the spectrum obtained from Eq. (30) includes quantum as well as classical dynamical effects through the evolution of the quantum proton in parallel with the classical evolution of the other nuclei and ADMP dynamics of the electrons.

#### 4 Future goals and generalizations

We have discussed a recently developed approach to perform efficient quantum dynamics of electronic and nuclear degrees of freedom. The salient features of the method include formally exact, accurate and efficient quantum dynamics using an analytic banded representation for the free propagator and efficient electronic dynamics using ADMP or Born–Oppenheimer dynamics. The quantum dynamics is performed using an analytic banded distributed approximating functional representation for the discretized free propagator and adaptive, interpolative grids are used to render an efficient implementation of wave-packet dynamics. One critical computational bottleneck in this approach involves the evaluation of the potential and forces on the discretized quantum grid. This is an important bottleneck in the current algorithm and is overcome using adaptive grids in conjunction with an importance sampling algorithm [56] that involves targeted potential sampling based on the local curvature, gradient information and wave-packet density. The result is used with multi-dimensional splines [56] to enhance the computational efficiency. While the quantum dynamics is currently performed using a third order Trotter factorization, the effect of other schemes will be studied in future publications. The electronic structure is treated accurately using hybrid or gradient corrected density functionals. State-of-the-art, higher order density functionals [91–93] can be easily included in the current scheme and such effects will be investigated as part of future studies. Furthermore, QM/MM generalization has also been recently demonstrated [57] and this should allow the treatment of large biological systems. Hence we envision that this approach will be useful to study quantum dynamics in large systems.

Many future methodological generalizations are planned. One area involves the calculation of infrared spectra of small clusters by including quantum dynamical effects of subsystems. Most current approaches dealing with large systems involve quantum corrections to classical dynamical correlation functions; the quantum corrections generally being obtained from within the harmonic approximation [137–139].

In the current formalism full quantum description of a portion of the system can be used in constructing a wave-packet averaged dipole correlation function, the Fourier transform of which would relate to the experimentally measured IR spectrum. This approach can be generalized to obtain other correlation functions as well. One bottleneck that we foresee in these calculations involves the matter of time scales; generally longer time-scale simulations are necessary to converge a dipole correlation function. This can be easily overcome for ADMP dynamics. This is because the only portions of the Fock matrix and gradients that need to be recomputed between grid points involve the one-electron term and this can be done easily. (The case for Born–Oppenheimer dynamics is more complicated and will require more work before we can achieve long-term dynamics.) Preliminary results to this effect have already been provided in this contribution.

A second area of study involves the extension of the quantum wavepacket AIMD to treat extended condensed phase systems. This kind of methodological generalization is important in many areas of chemical physics, for example, proton transport in polymer electrolyte membrane fuel cells [140–143], considered in hydrogen fuel cell applications. There will be two components to the methodological generalization that we will accomplish. Firstly, the quantum free-evolution operator in Eq. (10) will be modified to allow quantum evolution in an infinite system. This will be achieved through a periodic generalization of quantum propagation scheme through the use of a symmetry adapted form of the DAF-quantum propagator that will allow  $k$ -space integration. The second component of method development involved is the modification of AIMD to operate within periodic boundary conditions including  $k$ -space integration. If Born–Oppenheimer dynamics is to be employed then the classical nuclear forces are essentially the same as those derived previously [144] for periodic electronic structure calculations. However, if ADMP is to be employed then each  $k$ -point has a different density matrix that needs to be idempotent and propagated using equations similar to Eq. (5). The density matrices are only coupled by the energy expression.

Another area of computational improvement involves the treatment of multiple quantum nuclei in full dimensionality in conjunction with electronic dynamics as treated here. We believe this problem will be alleviated to some extent based on recent developments involving importance sampling [56]. Modified Neuman boundary conditions are also being used to achieve greater accuracy during wave-packet dynamics. QM/MM generalizations to the current approach are also underway.

The steps indicated above will lead to more efficient wave-packet dynamics schemes on a single potential energy surface. We are also currently working on generalizations to multiple electronic surfaces. These will involve two steps: (a) coupled ADMP dynamics of single particle density matrices leading to instantaneous approximations to the multiple electronic surfaces, and (b) quantum wave-packet dynamics on these coupled set of surfaces. These features will lead to many interesting studies in future.

**Acknowledgements** This research was supported by the Camille and Henry Dreyfus New Faculty Award Program and the Indiana University, Chemistry department. SSI is a Camille and Henry Dreyfus New Faculty Awardee. This paper has benefited from the contributions of my students and post-doc: Jacek Jakowski, Xiaohu Li, and Isaiah Sumner. In addition, the reviewer is duely acknowledged for excellent suggestions.

## References

- Wyatt RE, Zhang JZH (eds) (1996) Dynamics of molecules and chemical reactions. Marcel Dekker Inc., New York
- Berne BJ, Ciccotti G, Coker DF (eds) (1997) Classical and quantum dynamics in condensed phase simulations. World Scientific,
- Schatz GC, Kupperman A (1976) *J Chem Phys* 65:4642
- Delos JB (1981) *Rev Mod Phys* 53:287
- Feit MD, Fleck JA (1982) *J Chem Phys* 78:301
- Kosloff R (1994) *Ann Rev Phys Chem* 45:145
- Leforestier C, Bisseling RH, Cerjan C, Feit MD, Freisner R, Guldberg A, Hammerich A, Jolicard D, Karrlein W, Meyer HD et al. (1991) *J Comput Phys* 94:59
- DeVries P (1988) *Nato ASI Ser B171*:113
- Jang HW, Light JC (1995) *J Chem Phys* 102:3262
- Althorpe SC, Clary DC (2003) *Annu Rev Phys Chem* 54:493
- Huang Y, Iyengar SS, Kouri DJ, Hoffman DK (1996) *J Chem Phys* 105:927
- Miller WH, Schwartz SD, Tromp JW (1983) *J Chem Phys* 79:4889
- Makri N (1991) *Comp Phys Comm* 63:389
- Cao J, Voth GA (1994a) *J Chem Phys* 100:5106
- Jang S, Voth GA (1999) *J Chem Phys* 111:2357
- Feit MD, Fleck JA (1983) *J Chem Phys* 79:301
- Feit MD, Fleck JA (1984) *J Chem Phys* 80:2578
- Kosloff D, Kosloff R (1983a) *J Comput Phys* 52:35
- Kosloff D, Kosloff R (1983b) *J Chem Phys* 79:1823
- Tal-Ezer H, Kosloff R (1984) *J Chem Phys* 81:3967
- Hartke B, Kosloff R, Ruhman S (1986) *Chem Phys Lett* 158:223
- Iyengar SS, Kouri DJ, Hoffman DK (2000) *Theor Chem Acc* 104:471
- Lill JV, Parker GA, Light JC (1982) *Chem Phys Lett* 89:483
- Light JC, Hamilton IP, Lill JV (1985) *J Chem Phys* 82:1400
- Colbert DT, Miller WH (1992) *J Chem Phys* 96:1982
- Huang Y, Kouri DJ, Arnold M, Thomas I, Marchioro L, Hoffman DK (1994) *Comput Phys Comm* 80:1
- Wang ISY, Karplus M (1973) *J Amer Chem Soc* 95:8160
- Leforestier C (1978) *J Chem Phys* 68:4406
- Car R, Parrinello M (1985) *Phys Rev Lett* 55:2471
- Bolton K, Hase WL, Peslherbe GH (1998) *Modern methods for multidimensional dynamics computation in chemistry.* (World Scientific, Singapore, 1998). Chap. Direct dynamics of reactive systems, p 143
- Schlegel HB, Millam JM, Iyengar SS, Voth GA, Daniels AD, Scuseria GE, Frisch MJ (2001) *J Chem Phys* 114:9758
- Deumens E, Diz A, Longo R, Öhrn Y (1994) *Rev Mod Phys* 66:917
- Hack MD, Truhlar DG (2000) *J Phys Chem A* 104
- Jasper AW, Zhu C, Nangia S, Truhlar DG (2004) *Faraday Discussions* 127:1
- Miller WH (2001) *J Phys Chem A* 105:2942
- Heller EJ (1975) *J Chem Phys* 62:1544
- Fiete GA, Heller EJ (2003) *Phys Rev A* 68:022112
- Hammes-Schiffer S, Tully J (1994) *J Chem Phys* 101:4657
- Martinez TJ, Ben-Nun M, Ashkenazi G (1996) *J Chem Phys* 104:2847
- Micha DA (1999) *J Phys Chem A* 103:7562
- Ben-Nun M, Quenneville J, Martinez TJ (2000) *J Phys Chem A* 104:5161
- Coe JD, Martinez TJ (2005) *J Am Chem Soc* 127:4560
- Martinez TJ, Levine RD (1996) *J Chem Phys* 105:6334
- Payne MC, Teter MP, Allan DC, Arias TA, Joannopoulos JD (1992) *Rev Mod Phys* 64:1045
- Marx D, Hutter J (2000) (John vonNeumann Institute for Computing, Julich, 2000), vol 1, chap Ab Initio Molecular Dynamics: Theory and Implementation, pp 301–449
- Schlegel HB (2003) *J Comp Chem* 24:1514
- Dirac PAM (1958) *The principles of quantum mechanics: vol 27 of The international series of monographs on Physics*, 4th edn. Oxford University Press, New York
- Frenkel J (1934) *Wave mechanics.* Oxford University Press, Oxford
- Remler DK, Madden PA (1990) *Mol Phys* 70:921
- Andersen HC (1980) *J Chem Phys* 72:2384
- Parrinello M, Rahman A (1980) *Phys Rev Lett* 45:1196
- Pavese M, Berard DR, Voth GA (1999) *Chem Phys Lett* 300:93
- Tuckerman ME, Marx D (2001) *Phys Rev Lett* 86:4946
- Chen B, Ivanov I, Klein ML, Parrinello M (2003) *Phys Rev Lett* 91:215503
- Iyengar SS, Jakowski J (2005) *J Chem Phys* 122:114105
- Jakowski J, Iyengar SS. *J Chem Phys* (Submitted)
- Iyengar SS, Jakowski J. *J Phys Chem A* (Submitted)
- Iyengar SS, Schlegel HB, Millam JM, Voth GA, Scuseria GE, Frisch MJ (2001) *J Chem Phys* 115:10291
- Hoffman DK, Nayar N, Sharafeddin OA, Kouri DJ (1991) *J Phys Chem* 95:8299
- Hoffman DK, Kouri DJ (1992) *J Phys Chem* 96:9631
- Kouri DJ, Huang Y, Hoffman DK (1995) *Phys Rev Lett* 75:49
- Marchioro TL II, Arnold M, Hoffman DK, Zhu W, Huang YH, Kouri DJ (1994) *Phys Rev E* 50:2320
- Hoffman DK, Arnold M, Kouri DJ (1992) *J Phys Chem* 96:6539
- Newton RG (1982) *Scattering theory of waves and particles.* Springer, Berlin Heidelberg New York
- Schlegel HB, Iyengar SS, Li X, Millam JM, Voth GA, Scuseria GE, Frisch MJ (2002) *J Chem Phys* 117:8694
- Iyengar SS, Schlegel HB, Voth GA, Millam JM, Scuseria GE, Frisch MJ (2002) *Israel J Chem* 42:191
- Iyengar SS, Schlegel HB, Voth GA (2003) *J Phys Chem A* 107:7269
- Rega N, Iyengar SS, Voth GA, Schlegel HB, Vreven T, Frisch MJ (2004) *J Phys Chem B* 108:4210
- Iyengar SS, Frisch MJ (2004) *J Chem Phys* 121:5061
- Goedecker S (1999) *Rev Mod Phys* 71:1085
- Scuseria GE (1999) *J Phys Chem A* 103:4782
- White CA, Head-Gordon M (1994) *J Chem Phys* 101:6593
- Costentin C, Saveant J-M (2004) *J Am Chem Soc* 126:14787
- Gerber RB, Buch V, Ratner MA (1982) *J Chem Phys* 77:3022
- Bisseling RH, Kosloff R, Gerber RB, Ratner MA, Gibson L, Cerjan C (1987) *J Chem Phys* 87:2760
- Tully JC (1998) *Faraday Discuss* 110:407
- Sakurai JJ (1994) *Modern quantum mechanics.* Addison-Wesley Publishing Company
- Madelung E (1926) *Z Phys* 40:322
- de Broglie L (1930) *An introduction to the study of wave mechanics.* E.P. Dutton and Company, Inc., New York
- de Broglie L (1926) *Compt rend* 183:447
- de Broglie L (1927a) *Compt rend* 184:273
- de Broglie L (1927b) *Compt rend* 185:380
- Bohm D (1952) *Phys Rev* 85:166
- Cushing JT, Fine A, Goldstein S (eds) (1996) *Bohmian mechanics: an appraisal.* Kluwer, Boston
- Holland PR (1993) *The quantum theory of motion.* Cambridge, New York
- Gindensperger E, Meier C, Beswick JA (2000) *J Chem Phys* 113:9369
- Prezhdo OV, Brooksby C (2000) *Phys Rev Lett* 86:3215
- Becke AD (1993) *J Chem Phys* 98:5648
- Becke AD (1988) *J Chem Phys* 88:3098
- Perdew JP, Burke K, Ernzerhof M (1996) *Phys Rev Lett* 77:3865
- Tao J, Perdew JP, Staroverov VN, Scuseria GE (2003) *Phys Rev Lett* 91:146401
- Zhao Y, Truhlar DG (2004) *J Chem Phys* 108:6908
- Zhao Y, Lynch BJ, Truhlar DG (2005) *Phys Chem Chem Phys* 7:43

94. McWeeny R (1960) *Rev Mod Phys* 32:335
95. Ehrenfest P (1927) *Z Phys* 45:455
96. Donoso A, Zheng YJ, Martens CC (2003) *J Chem Phys* 119:5010
97. Kapral R, Ciccotti G (1999) *J Chem Phys* 110:8919
98. Wigner EP (1932) *Phys Rev* 40:749
99. Trotter MF (1959) *Proc Am Math Soc* 10:545
100. Strang G (1968) *SIAM J Numer Anal* 5:506
101. Nelson E (1964) *J Math Phys* 5:332
102. Neuhauser D (1991) *J Chem Phys* 95:4927
103. Arfken G (1985) *Mathematical methods for physicists*. Academic Press, New York
104. Mowrey RC, Kouri DJ (1986) *J Chem Phys* 84:6466
105. Feynman RP, Hibbs AR (1965) *Quantum mechanics and path integrals*. McGraw-Hill Book Company, New York
106. Schulman LS (1986) *Techniques and applications of path integration*. Wiley, New York
107. Chandler D, Wolynes PG (1981) *J Chem Phys* 74:4078
108. Berne BJ, Thirumalai D (1986) *Annu Rev Phys Chem* 37:401
109. Cao J, Voth GA (1994b) *J Chem Phys* 100:5093
110. Hoffman DK, Marchioro TL, Arnold M, Huang YH, Zhu W, Kouri DJ (1996) *J Math Chem* 20:117
111. Hoffman DK, Wei GW, Zhang DS, Kouri DJ (1998) *Phys Rev E* 57:6152
112. Hoffman DK, Wei GW, Kouri DJ (1999) *J Math Chem* 25:235
113. Korevaar J (1959) *Pansions and the theory of Fourier transforms*. Amer Math Soc Trans
114. Yu S, Zhao S, Wei GW (2005) *J Comput Phys*
115. Abramowitz M, Stegun IA (eds) (1964) *Handbook of mathematical functions*. U.S. GPO, Washington, D.C.,
116. Billing GD (2001) *J Chem Phys* 114:6641
117. Grossman A, Morlet J (1984) *SIAM J Math Anal* 15:723
118. Strang G (1989) *SIAM Review* 31:613
119. Daubechies I (1992) *Ten lectures in wavelets*. SIAM, Philadelphia
120. Strang G, Nguyen T (1996) *Wavelets and filter banks*. Wellesley-Cambridge Press
121. Klauder JR, Skagerstam B-S (1985) *Coherent states: applications in physics and mathematical physics*. World Scientific Publishing Company, Inc.
122. Klauder JR, Daubechies I (1984) *Phys Rev Lett* 52:1161
123. Zhao Y, Yokojima S, Chen G (2000) *J Chem Phys* 113:4016
124. Morales J, Deumens E, Ohrn Y (1999) *J Math Phys* 40:766
125. Goldstein H (1980) *Classical mechanics*. Addison-Wesley Press, Cambridge, Massachusetts
126. Riesz F, Sz-Nagy B (1990) *Functional analysis*. Dover Publications, Inc., New York
127. Golub GH, van Loan CF (1996) *Matrix computations*. The Johns Hopkins University Press, Baltimore
128. Iyengar SS, Petersen MK, Day TJJ, Burnham CJ, Teige VE, Voth GA (2005) *J Chem Phys* 123:084309
129. Iyengar SS, Day TJJ, Voth GA (2005) *Int J Mass Spectrometry* 241:197
130. Petersen MK, Iyengar SS, Day TJJ, Voth GA (2004) *J Phys Chem B* 108:14804
131. Kouri DJ, Hoffman DK (2000) *Phys Rev Lett* 85:5263
132. Chandler C, Gibson A (1999) *J Approx Theory* 100:233
133. Iyengar SS, Parker GA, Kouri DJ, Hoffman DK (1999) *J Chem Phys* 110:10283
134. Bender CM, Orzag SA (1978) *Advanced mathematical methods for scientists and engineers*. McGraw-Hill Publishing Company, New York
135. Marcus RA (1993) *Rev Mod Phys* 65:599
136. Kaledin M, Brown A, Kaledin AL, Bowman JM (1964) *Phys Rev* 136:A405
137. Berens PH, White SR, Wilson KR (1981) *J Chem Phys* 75:515
138. Bader JS, Berne BJ (1994) *J Chem Phys* 100:8359
139. Lawrence CP, Nakayama A, Makri N, Skinner JL (2004) *J Chem Phys* 120:6621
140. Schuster MF, Meyer WH (2003) *Annu Rev Mat Res* 33
141. Kreuer KD, Fuchs A, Ise M, Spaeth M, Maier J (1998) *Electrochimica Acta* 43
142. Schuster MF, Meyer WH (2004) *J Phys Chem B* 108
143. Iannuzzi M, Parrinello M (2004) *Phys Rev Lett* 93
144. Kudin KN, Scuseria GE (2000) *Phys Rev B* 61:16440